www.MaterialsViews.com

ADVANCED
FUNCTIONAL
MATERIALS
www.afm-journal.de

FULL PAPER

A Universal and Facile Approach for the Formation of a Protein Hydrogel for 3D Cell Encapsulation

Yin Chen, Xin Dai, Lu Huang, Yang Sun, Ho N. Chan, Bo Shen, Xiaoqian Zeng, Zhenguo Wu, I-Ming Hsing, Zhihong Guo, and Hongkai Wu*

A universal and facile approach to modifying proteins so that they can rapidly form hydrogel upon mixing with crosslinkers is presented. The concept of it is to introduce maleimide, which is highly reactive with dithiol-containing crosslinkers via thiol-ene click chemistry, onto proteins. Bovine serum albumin (BSA) is used as a model protein due to its good stability and low cost. The results here show that a protein hydrogel can be readily formed by blending modified BSA and resilin-related peptide crosslinker solutions at a proper ratio. The hydrogel exhibits good elasticity and tunable mechanical as well as biochemical properties. Moreover, it allows convenient 3D cell encapsulation and shows good biocompatibility. Muscle cells embedded in the hydrogel are promoted to spread by incorporating arginyl-glycyl-aspartic acid (RGD)-containing peptide into the system, thus warranting a bright future of it in regenerative medicine.

1. Introduction

In the past few years, the fast progresses in tissue engineering and the emergency of 3D bioprinting have brought new hope in regenerative medicine.[1] For the first time in history, mankind seems to have grasped the power to configure a complex tissue or even an integrated organ using the bottom-up approach.[1c–e] In order to engineer artificial tissues or even organs, various types of cells with distinct biological functions are required.[2] Another indispensable component is a competent scaffold material, which can support the encapsulation, growth, migration and remodeling of cells.[1a,b,2,3] Although great achievements in stem cell technology have enabled us to obtain unlimited numbers of differentiated cells for tissue-regenerating purpose,[4] challenges still remain in developing adequate scaffold materials due to the complexity of native tissues and organs.[1a,5] There is no universal scaffold material in tissue engineering only in view of the wide variations in the mechanical property among different tissues, whose stiffness alone may range from <100 Pa to >10 GPa.[6] A longstanding point in the choice of scaffold material for tissue engineering is that the material itself must have a matched mechanical property as the specific tissue to be created.[7] Besides, it is expected to facilitate cell encapsulation, possess good biocompatibility, and allow degradation or remodeling by cells as mentioned before.[1b–3]

Hydrogel is an ideal class of materials for tissue engineering owing to its similarities to natural extracellular matrix (ECM), thus providing cells with physical and biochemical cues resembling those of their native environment.[8] Among this class of materials, protein hydrogel has attracted a lot of interest thanks to many self-evident advantages, such as good biocompatibility, tunable mechanical property, and facile bioactive ligand incorporation.[3,9] To date, diverse crosslinking methods have been developed for protein hydrogel.[10] However, great limitations still exist in their application, such as weak mechanical strength for physical crosslinking and harsh reaction conditions as well as slow gelation rate for photochemical crosslinking.[10a–d] Therefore, new means for the curing of protein hydrogel that overcome the drawbacks mentioned above are in urgent need.

Herein, we present a universal and facile approach to modifying proteins so that they can rapidly form hydrogel upon mixing with crosslinkers. The concept of it is to introduce maleimide onto proteins, which is highly reactive with dithiol-containing crosslinkers via thiol-ene click chemistry.[11] In our study, bovine serum albumin (BSA) was used as a model protein on account of its good stability and low cost. Besides, its secondary structure might function as an energy absorber through unfolding, thus conferring the BSA-based hydrogel good toughness. The crosslinker applied is a resilin-related peptide (RRP) composed of a frequently repeated sequence in resilin and flanked with two cysteine residues (**Figure 1**). Resilin is a rubber-like protein found in the cuticle of most insects, which is well-known for its role in the remarkable

Y. Chen, L. Huang, Prof. I.-M. Hsing, Prof. H. Wu
Division of Biomedical Engineering
The Hong Kong University of Science and Technology
Hong Kong, China
E-mail: chhkwu@ust.hk
X. Dai, L. Huang, H. N. Chan, B. Shen,
Prof. Z. Guo, Prof. H. Wu
Department of Chemistry
The Hong Kong University of Science and Technology
Hong Kong, China
Y. Sun, Prof. Z. Wu
Department of Life Science
The Hong Kong University of Science and Technology
Hong Kong, China
X. Zeng
Laboratory Department
Union Hospital of Tongji Medical College
Huazhong University of Science and Technology
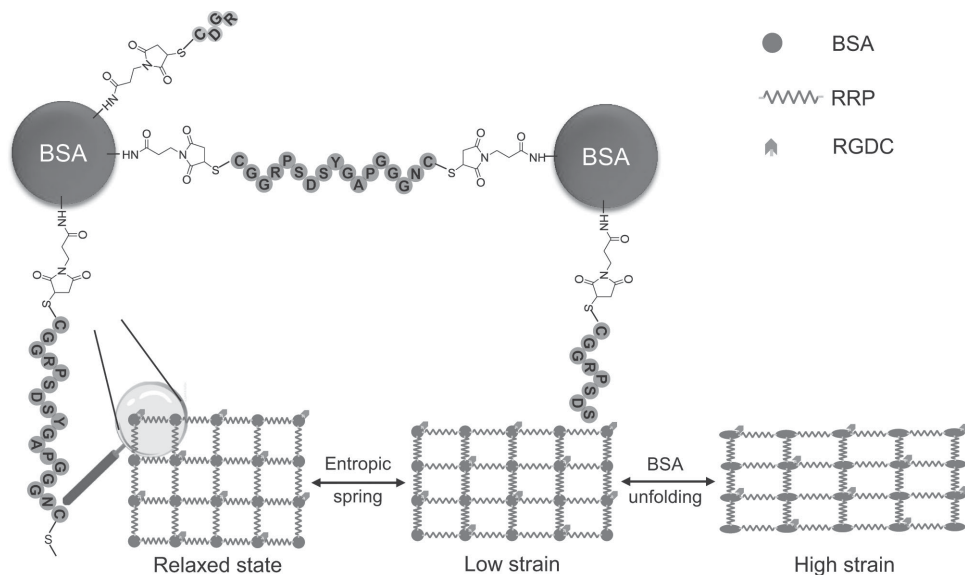Wuhan 430022, China

Figure 1. Putative structure for the bovine serum albumin (BSA)-based protein hydrogel network. BSA is crosslinked by click chemistry between maleimide on it and thiol on the resilin-related peptide (RRP). At a low strain, RRP functions as an entropic spring to confer the hydrogel good elasticity while at a high strain, BSA unfolding works as an energy absorber to make the hydrogel stretchable. RGD-containing peptide could also be readily incorporated with the same click chemistry to promote cell adhesion in the hydrogel.

jumping ability and flight of insects as a result of its high elasticity and resilience.[12] Although the mechanism on the high elasticity and resilience of resilin is still under investigation,[13] it is hypothesized that the protein hydrogel network generated by the click chemistry between maleimide-modified BSA and dithiol-functionalized RRP would be elastic and stretchable. In addition, bioactive ligands such as arginyl-glycyl-aspartic acid (RGD)-containing peptide for promoting cell adhesion could be handily incorporated.[14]

2. Results and Discussion

2.1. Maleimidyl Modification on BSA

Through reaction with *N*-(β-maleimidopropyloxy)succinimide ester (BMPS) (Figure S1, Supporting Information), maleimidyl groups were successfully conjugated onto BSA as corroborated by proton nuclear magnetic resonance (¹H-NMR) (**Figure 2**a). The number of it on BSA can be fine-tuned by the molar feed ratio of BMPS to BSA during the coupling reaction. First of all, we studied the influence of maleimidyl modification on the structure of BSA. Dynamic light scattering (DLS) (Figure 2b) unravels that the size of BSA increases in accordance with the degree of modification (DM). This result suggests the formation of agglomerates generated by BSA monomers. To confirm the nature of the interaction between the BSA monomers, sodium dodecyl sulfate polyacrylamide gel electrophoresis (SDS-PAGE) was performed and our result (Figure 2c) unveils the covalent bonding between them. Indeed, ¹H-NMR indicates the presence of Schiff base due to the reaction between amine from amino acid residues and carbonyl on maleimide. Moreover, Michael-type addition was also found to occur between amine and double bond. It is likely that BSA oligomers were

produced because of these chemical reactions. To our surprise, whatever DM is, no prominent change in the secondary structure of BSA was observed as revealed by the circular dichroism (CD) spectroscopy (Figure 2d and Table S1, Supporting Information), which is a clear evidence for its excellent conformational stability.

2.2. Gelation Formulations for BSA Solution

The gelation formulations for BSA solutions using RRP as the crosslinker were systematically investigated (**Figure 3**). Pristine, dialyzed or modified BSA was prepared as a solution (100 mg mL⁻¹ in 100 × 10⁻³ M Na₂HPO₄, pH ≈ 7.5) and mixed with RRP solution (100 mg mL⁻¹ in 140 × 10⁻³ M NaOH solution, pH ≈ 7.5) at varying volume ratios. As anticipated, unmodified BSA is unable to form a hydrogel at any formulations. In addition, BSA-BMPS(3.2) solution could not solidify either as a result of the small number of maleimidyl groups conjugated on it. Increasing the amount of maleimidyl groups on BSA makes the gelation possible and the higher DM of it allows the protein solution to be cured in a wider range of formulations with the peptide crosslinker. Nonetheless, we must point out that when the DM is too high, gelation could not happen at the highest ratio (9:1) of BSA to RRP tested here, as evidenced by BSA-BMPS(16.5) and BSA-BMPS(14.7). This is because that the chance is better for both sulfhydryl groups of a crosslinker peptide molecule to react with maleimidyl groups on the same BSA molecule at such case, forming mainly intramolecular crosslinking. In fact, a proper ratio of BSA to RRP is required in order to form a stable hydrogel. At a lower ratio of BSA to RRP, many crosslinker molecules would only react with BSA using one of their sulfhydryl groups owing to the excessive amount of them, without generating sufficient intermolecular crosslinking
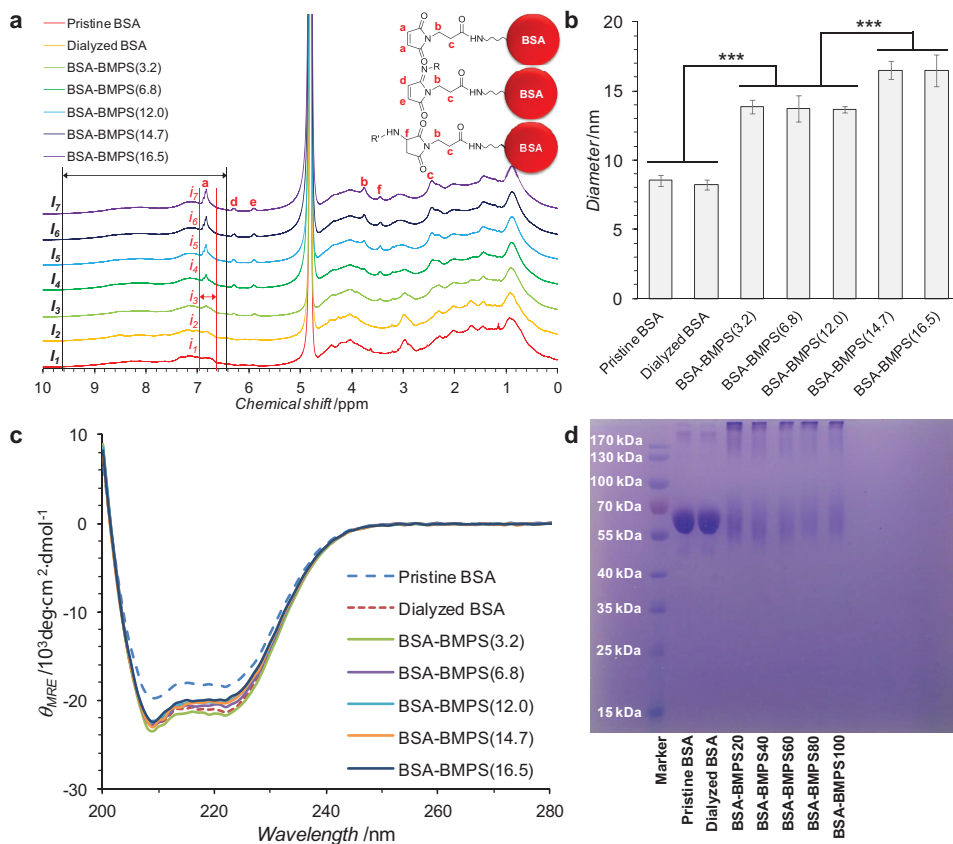
www.MaterialsViews.com

ADVANCED
FUNCTIONAL
MATERIALS
www.afm-journal.de

FULL PAPER

Figure 2. Characterization on the maleimidyl modification on BSA. a) Proton nuclear magnetic resonance (^{1}H-NMR) spectra of pristine and modified BSA. The assignment of peaks related to the modification of BSA is given. The spectra reveal the presence of a Schiff base due to the reaction between amines from amino acid residues and carbonyls on maleimidyl groups. Moreover, Michael-type addition is also found to occur between amine and double bond. Spectra were normalized by setting the height of the peak between 0.9 and 1.0 ppm to be 1000 and were offset for display. The degree of maleimidyl modification on BSA was computed based on the number of aromatic protons in it. The details for the computation are given in the Supporting Information. b) Dynamic light scattering (DLS) unravelling the increase in size (mean ± sem, $n \geq 12$, ***$P < 0.001$) of BSA after modification. Figures in the brackets indicate the mean number of maleimidyl groups conjugated on each BSA molecule. c) Circular dichroism (CD) spectroscopy showing no prominent change in the secondary structure of BSA. d) Sodium dodecyl sulfate polyacrylamide gel electrophoresis (SDS-PAGE) for pristine and modified BSA. The leftmost column is the prestained protein ladder marker, for which the molecular weights of individual proteins are designed according to the instructions provided by the manufacturer. Substantial amounts of protein agglomerates were generated in modified BSA as unraveled by SDS-PAGE due to the chemical reactions between the protein monomers.

either. In consistency with our expectation, the lowest ratio of BSA to RRP that permits gelation to occur declines with the increase in DM of BSA. The formulations which have potential for 3D cell encapsulation (i.e., those form hydrogel within 1 h or become viscous within 1 h and form hydrogel within 12 h) are defined by an enclosed dashed line in Figure 3. Except for BSA-BMPS(6.8) and BSA-BMPS(12.0) at 9:1 ratio of BSA to RRP, hydrogel could be formed within one hour.

2.3. Stiffness of BSA-Based Hydrogels

Since a lot of research has proved the pivotal role played by the stiffness of ECM in the fate and/or behavior of cells encapsulated in or cultured on it,[7a],[15] we examined the stiffness of BSA-based hydrogels formed from the formulations (Figure 3) that have potential for 3D cell encapsulation by shear test. Our results (**Figure 4**) demonstrate that the stiffness (mainly reflected

by the storage modulus) of hydrogel could be altered from <100 Pa to >5000 Pa by adjusting DM of BSA or the ratio of BSA to RRP, which covers the scope of soft tissues such as nerve, fat and muscle.[6] In particular, the stiffness of protein hydrogel is strongly dependent on the ratio of BSA to RRP when DM of BSA is fixed. In general, the maximum mechanical strength is achieved at an intermediate value of it. As mentioned above, both high proportion of BSA and that of RRP are detrimental for the formation of intermolecular crosslinking between BSA molecules. Correspondingly, only at an optimal ratio of BSA to RRP could a mechanically strong hydrogel be acquired, as illustrated in Figure S2, Supporting Information. As a matter of fact, one of our objectives is to fabricate a 3D artificial cardiac tissue for the treatment of myocardial infarction, which is a common modality of heart diseases that is hard to tackle due to the lack of regenerative capability of native myocardium. Among all the formulations of hydrogel, BSA-BMPS(12.0):RRP = 8:2, BSA-BMPS(14.7):RRP = 8:2, and BSA-BMPS(16.5):RRP = 7:3 have
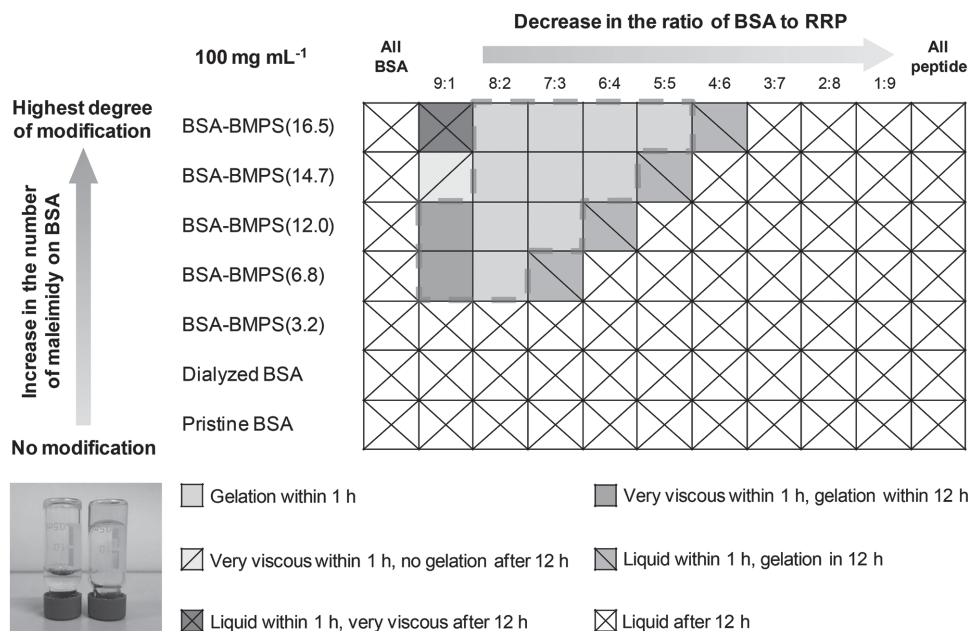
Figure 3. Phase diagram summarizing gelation formulations for BSA-based hydrogel using RRP as the crosslinker. The degree of maleimidyl modification on BSA increases with the molar feed ratio of N-(β-maleimidopropyloxy)succinimide ester (BMPS) to BSA during the coupling reaction. Pristine or modified BSA was prepared as a solution (100 mg mL^{-1} in 100×10^{-3} M Na$_2$HPO$_4$, pH $\approx$ 7.5) and mixed with RRP solution (100 mg mL^{-1} in 140×10^{-3} M NaOH solution, pH $\approx$ 7.5) at varying volume ratios. The picture at the left corner shows BSA solution (Dialyzed BSA:RRP = 9:1) and hydrogel (BSA-BMPS(16.5):RRP = 8:2).
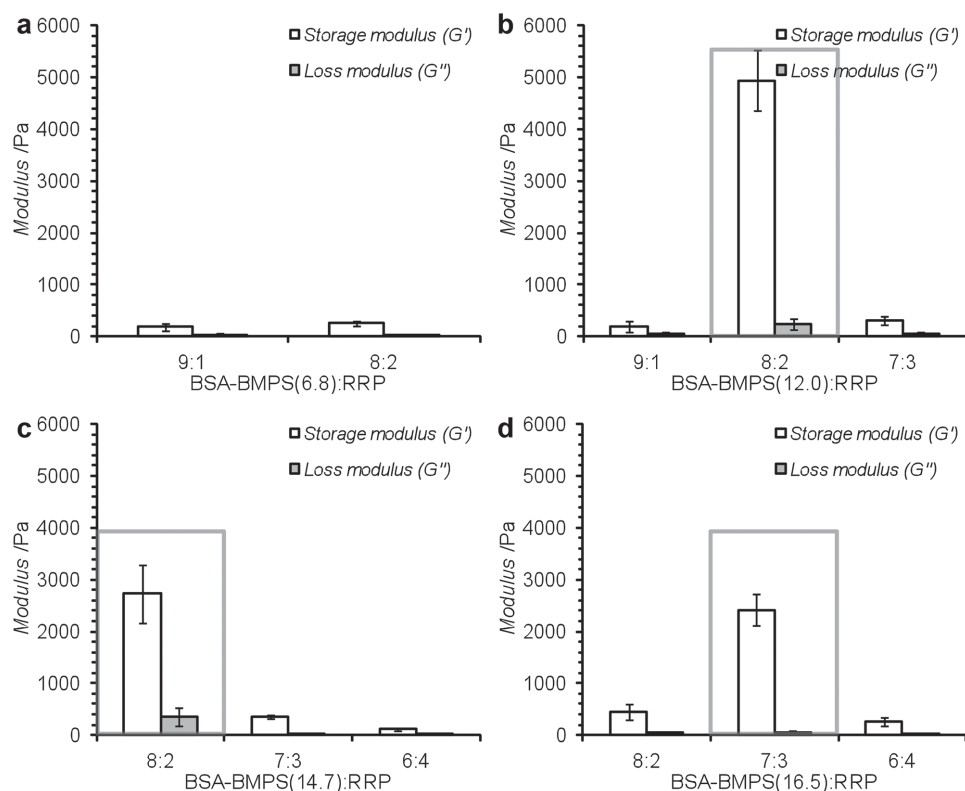

Figure 4. Stiffness (mean $\pm$ std, $n \geq 5$) of BSA-based hydrogels formed from the formulations (except for BSA(16.5):RRP = 5:5 which is too weak to be measured) with potential for 3D cell encapsulation measured by shear test. The measurements were performed at 5% strain and 10 rad s^{-1} frequency. Among all the formulations of the hydrogel, those highlighted within rectangular boxes have exhibited muscle-like stiffness.

BSA-BMPS(12.0):RRP = 8:2   BSA-BMPS(14.7):RRP = 8:2   BSA-BMPS(16.5):RRP = 7:3
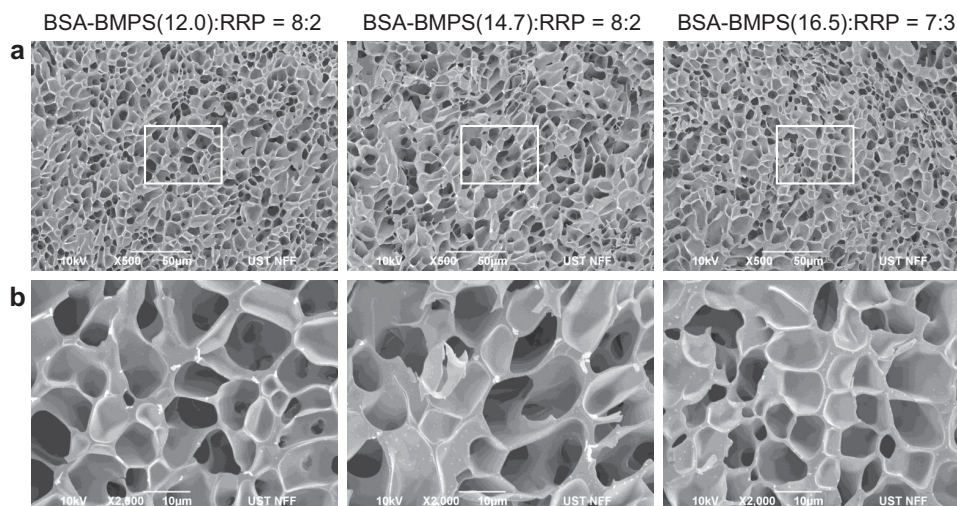

Figure 5. Scanning electron microscopy (SEM) images showing the inner morphologies of the three representative hydrogels whose stiffness is comparable to that of native muscle tissue. Images in (b) display the magnified details of encompassed regions in (a). Homogenous porous structures with similar pore sizes and distributions among the three hydrogels are observed. (Scale bars: 50 μm in (a) and 10 μm in (b))

exhibited muscle-like stiffness.[6] Besides, these three formulations could rapidly form hydrogel within one minute at physiological pH and ambient temperature, which are appropriate for 3D cell encapsulation. Because of these concerns, our following work is focused on these three hydrogels.

2.4. Inner Structures and Swelling Behaviors of Hydrogels

We examined the inner structures of freeze-dried hydrogels with scanning electron microscopy (SEM), which disclosed homogenous porous structures with similar pore sizes and distributions among the three representative hydrogels (**Figure 5**). However, for those hydrogels with a stiffness one magnitude lower, looser structures with larger pore sizes were observed (Figure S3, Supporting Information). Water uptake capability, which is an index characterizing swelling of cured hydrogel in aqueous solutions such as PBS and cell culture medium, increases as the decrease in stiffness of hydrogels, though the values for all the tested formulations are small (<30% in PBS, pH ≈ 7.4, Figure S4, Supporting Information). These results imply that softer hydrogels have lower crosslinking densities and may be less stable as scaffold materials for long-term 3D cell culture.

2.5. Dynamic and Static Mechanical Behavior of Hydrogels

To better understand the mechanical properties of our hydrogels, we further inspected the rheological behaviors of them at strain and frequency sweep modes, respectively. As controls, hydrogels of BSA-BMPS(12.0) were also prepared by using dithiothreitol (DTT, dissolved in PBS, pH ≈ 7.4) as the crosslinker at the same volume ratio of 8:2. As shown in **Figure 6**, all the three representative hydrogels display outstanding elasticity at a low strain (<5%) as evidenced by the dominance of storage modulus (G') over loss modulus (G''). Afterwards, they gradually lose their elasticity as the G'' becomes domi-

nant at a larger strain. At a low strain, BSA-BMPS(12.0):RRP = 8:2 presents the highest stiffness (G' = 4.9 ± 0.6 kPa) while the other two hydrogels possess comparable stiffness (G' = 2.7 ± 0.6 kPa for BSA-BMPS(14.7):RRP = 8:2 and G' = 2.4 ± 0.3 kPa for BSA-BMPS(16.5):RRP = 7:3), which might be explained by the highest intermolecular crosslinking density in BSA-BMPS(12.0):RRP = 8:2. To examine our observations, we also performed tensile test. The stress-strain plot delineates a linear relationship even up to the strain at breakage (ε_b) for all the hydrogels (**Figure 7**). In agreement with the dynamic mechanical analysis, tensile test (**Table 1**) demonstrates BSA-BMPS(12.0):RRP = 8:2 has the largest Young's modulus (22.0 ± 1.9 kPa) while the moduli for the other two hydrogels are close (12.0 ± 1.2 kPa for BSA-BMPS(14.7):RRP = 8:2 and 10.4 ± 0.7 kPa for BSA-BMPS(16.5):RRP = 7:3). Unfortunately, none of them are highly stretchable and all of them break at a strain less than 50%. Surprisingly, the Young's moduli, strains at breakage and stresses at breakage of BSA-BMPS(12.0):DTT(6.5 mg mL^{-1}) = 8:2 and BSA-BMPS(12.0):DTT(6.0 mg mL^{-1}) = 8:2 were close to those of BSA-BMPS(12.0):RRP = 8:2 and BSA-BMPS(14.7):RRP = 8:2, respectively. Based on these results, it can be concluded that BSA was hardly unfolded during the mechanical tests and it is the random coils of BSA that make the major contribution to the good elasticity and limited extensibility of the hydrogels. This could be attributed to the rigidity of BSA as a result of seventeen intramolecular disulfide bonds in it.[16] RRP could also have contributed to the elasticity and extensibility of BSA though it might be minor as BSA-BMPS(16.5):RRP = 7:3 exhibits the best extensibility with a ε_b of 47.9 ± 4.4%. Higher extensibility of the protein hydrogel might be realized by breaking off the intramolecular disulfide bonds in BSA and/or by extending the length of crosslinker to be used.

Normally, the increase in crosslinking density within a polymeric hydrogel will lead to the increase in stiffness while in the meantime the reduction in yield strain. Although the stiffness of BSA-BMPS(12.0):RRP = 8:2 is almost two-fold as
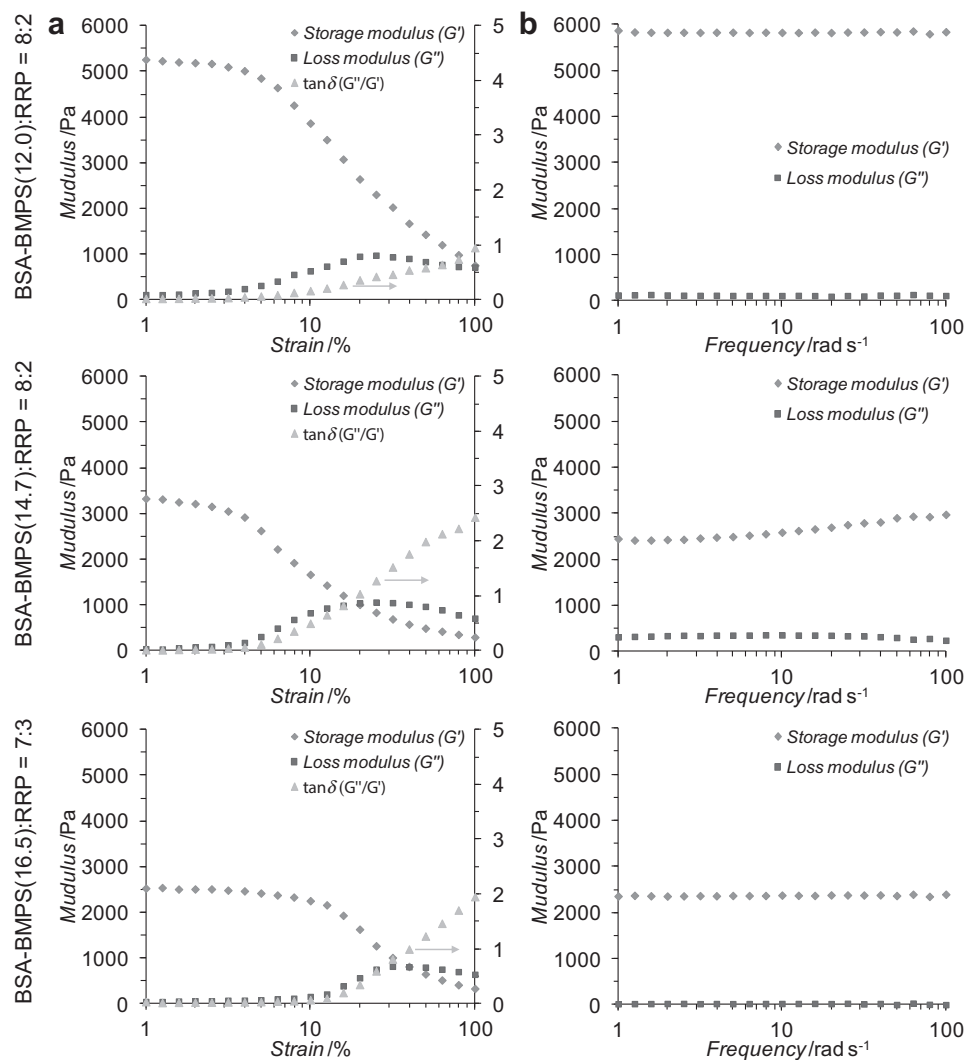
FULL PAPER

Figure 6. Dynamic mechanical analysis (DMA) on the BSA-based hydrogels formed from the three representative formulations. The measurements were performed at a) strain sweep mode (1% to 100% strain at 10 rad s^{-1} frequency) and b) frequency sweep mode (1 to 100 rad s^{-1} frequency at 5% strain).

that of BSA-BMPS(14.7):RRP = 8:2, the former hydrogel shows a significantly ($P < 0.01$) larger ε_b (35.4 ± 3.4%) than the latter one (28.4 ± 2.9%). Similar trend is also discovered by rheological study, which reveals that BSA-BMPS(12.0):RRP = 8:2 displays a higher strain at $G''/G' = 0.1$ ($\gamma_{\tan\delta} = 0.1$, Figure S4.7, Supporting Information) (8.9 ± 2.1%) than that (4.9 ± 1.6%) of BSA-BMPS(14.7):RRP = 8:2. Moreover, the measurements carried out at frequency sweep mode corroborate the good elasticity

of both BSA-BMPS(12.0):RRP = 8:2 and BSA-BMPS(16.5):RRP = 7:3 but fair elasticity of BSA-BMPS(14.7):RRP = 8:2 at 5% strain. The G''s of the former two hydrogels are negligible while the G's of them are almost constant within the range of shear frequency tested (1 to 100 Hz), which are the characteristic features of elastic materials. In contrast, for the rest hydrogel G'' is large initially (>300 Pa) and it decreases with frequency while G' increases with it, which is suggestive of its notable viscosity.

Table 1. Mechanical properties (mean ± std, $n \geq 6$) of the hydrogels from tensile test.

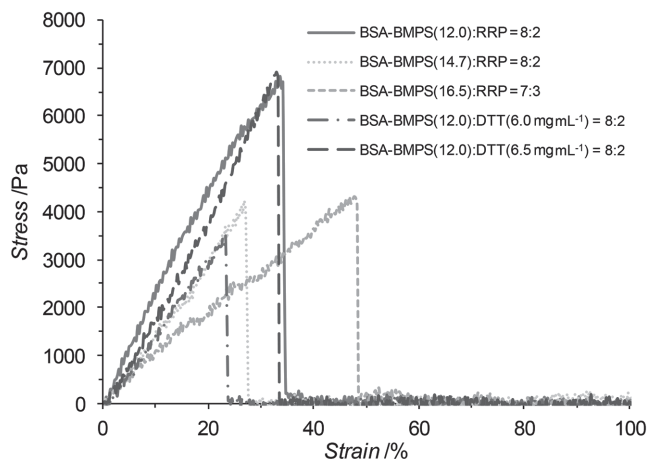| Formulation of hydrogel	Young's modulus (E_Y) [kPa]	Strain at breakage (ε_b) [%]	Stress at breakage (σ_b) [kPa]
BSA-BMPS(12.0):RRP = 8:2	22.0 ± 1.9	35.4 ± 3.4	6.7 ± 0.7
BSA-BMPS(14.7):RRP = 8:2	12.0 ± 1.2	28.4 ± 2.9	3.9 ± 0.4
BSA-BMPS(16.5):RRP = 7:3	10.4 ± 0.7	47.9 ± 4.4	4.6 ± 0.5
BSA-BMPS(12.0):DTT(6.0 mg mL^{-1}) = 8:2	12.9 ± 1.6	24.5 ± 3.9	3.6 ± 0.4
BSA-BMPS(12.0):DTT(6.5 mg mL^{-1}) = 8:2	17.8 ± 2.3	34.2 ± 4.3	6.4 ± 0.9

Figure 7. Stress-strain plot for the three representative hydrogels and two BSA-based hydrogels cured by using dithiothreitol (DTT). The plot delineates a linear relationship even up to the strain at breakage (ε_b) for all the hydrogels tested.

It is worthy to note that G' is likely to represent the entropic springs of RRP and random coils in BSA while G'' reflects the unfolding of secondary structures in protein though the degree of it is very limited. At a high shear frequency, the unfolding of secondary structures becomes less prominent and they behave more like random coils. Interestingly, the same phenomenon is also observed in the control group (Figures S5 and S6, Supporting Information), for which BMPS(12.0):DTT(6.5 mg mL^{-1}) = 8:2

shows a higher stiffness with a larger ε_b and $\gamma_{\tan\delta} = 0.1$ than BSA-BMPS(12.0):DTT(6.0 mg mL^{-1}) = 8:2. These behaviors must be ascribed to the unique molecular structure of BSA-based hydrogel, which is formed by the crosslinking between BSA oligomers that could be regarded as "nanogels". According to the observations, the mechanical properties such as viscoelasticity and yield strain of the hydrogels are mainly determined by those BSA nanogels. At a higher ratio of maleimidyl groups over sulfhydryl groups as to BSA-BMPS(14.7):RRP = 8:2 or BSA-BMPS(12.0):DTT(6.0 mg mL^{-1}) = 8:2, the crosslinker would preferentially induce intramolecular crosslinking within the nanogels, thus leading to both a lower stiffness and a smaller yield strain simultaneously.

2.6. 3D Cell Encapsulation

As our protein hydrogel had been developed for muscle regeneration, we tested its potential as a 3D cell culture matrix. C2C12, a widely used muscle cell line, was embedded in the hydrogel by mixing BSA-BMPS(12.0) solution (100 mg mL^{-1}) containing cells (10^6 cells mL^{-1}) with crosslinker solution (100 mg mL^{-1} RRP or 98 mg mL^{-1} RRP plus 2 mg mL^{-1} RGDC) at a volume ratio of 8:2. After incubation for one week, live/dead cell staining was performed and we found that more than 85% cells were still alive (**Figure 8**a), demonstrating good biocompatibility of our material. Unfortunately, cells could hardly spread within the hydrogel without cell-adhesive ligands and some might have died of apoptosis. However, by incorporating
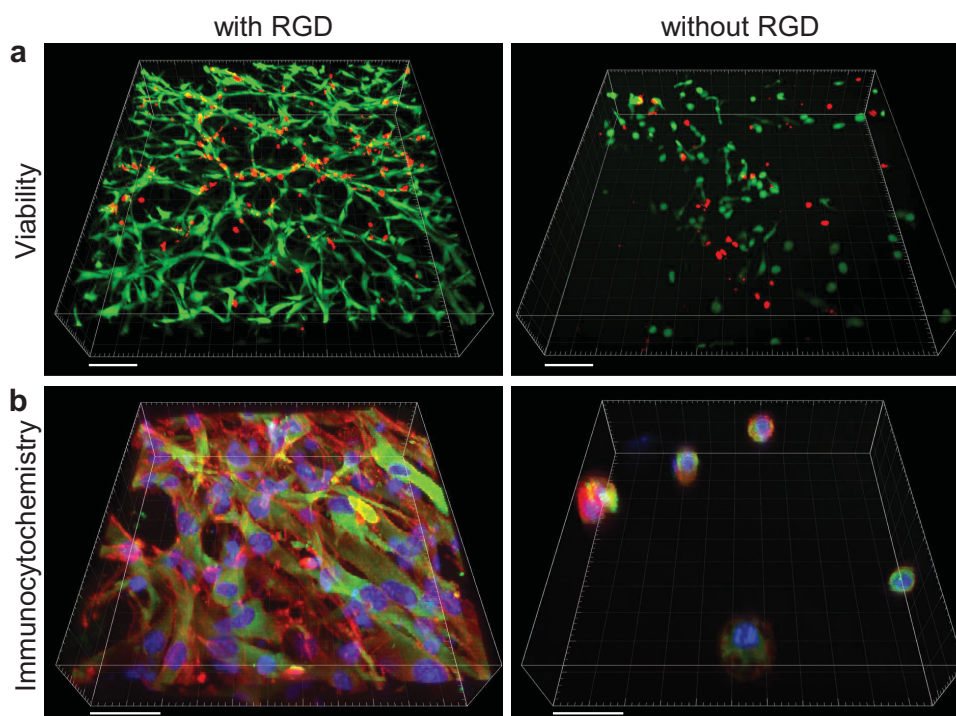

Figure 8. Confocal laser scanning microscopy (CLSM) revealing a) the viability and b) immunostaining of C2C12 skeletal muscle cells in the protein hydrogel matrix with and without the presence of RGD-containing peptide. a) Live cells were stained in green (FDA) while dead ones in red (PI). b) F-actin was stained in red, sarcomeric α-actinin in green and cell nuclei in blue. (Scale bars: 100 µm in (a) and 50 µm in (b))

bioactive ligand such as RGD, they could fully spread in the 3D environment and even proliferate as proved by the much higher density. Indeed, cells in the hydrogel with RGD showed higher viability than those in the matrix without it (95 ± 2% vs 86 ± 4%, $P < 0.05$, $n = 3$), probably due to the proliferation of them. Immunostaining (Figure 8b) revealed the expression of sarcomeric α-actinin by cells in both groups though they could hardly spread without RGD, which implied C2C12 could maintain its lineage commitment in our hydrogel without differentiating into other types of cells such as osteoblast.

3. Conclusion

In summary, we have presented a simple approach to modifying BSA so that it can rapidly form a hydrogel upon mixing with dithiol-containing crosslinkers via thiol-ene click chemistry. It should be pointed out that this approach is universal to other proteins such as collagen and gelatin (data not presented) as long as the protein has sufficient numbers of amino groups. In our study, the BSA-based protein hydrogel has shown good elasticity at a low strain, and its stiffness can be fine-tuned by the degree of maleimidyl modification on BSA and the mass ratio of BSA to RRP. Although its stretchability is poor because of the high rigidity of BSA and the short length of RRP used here, the protein hydrogel allows facile 3D cell encapsulation and possesses good biocompatibility. More importantly, bioactive ligands such as RGD-containing peptide can be readily incorporated as demonstrated, which will enhance the adhesion, spreading, growth, and even differentiation of cells. Future work will be to improve the toughness of our protein hydrogel by breaking the seventeen intramolecular disulfide bonds of BSA and using RRP with longer chains.

4. Experimental Section

Materials: BSA (Cat. No.: A7906), Dulbecco's modified Eagle's medium (DMEM, Cat. No.: D7777), fluorescein diacetate (FDA, Cat. No.: F7378) and propidium iodide (PI, Cat. No.: P4170) were purchased from Sigma-Aldrich. Resilin-related peptide (RRP, sequence: CGGRPSDSYGAPGGGNC, purity >90%) and RGD-containing peptide (sequence: RGDC, purity >95%) were synthesized by ChinaPeptides (Suzhou, China). Fetal bovine serum (FBS, Cat. No.: 26140–079), horse serum (HS, Cat. No.: 16050–114), penicillin/streptomycin (P/S, Cat. No.: 15140), rhodamine-labeled phalloidin (Cat. No.: R415) and 4′,6-diamidino-2-phenylindole diacetate (DAPI, Cat. No.: D3571) were provided by Life Technologies. Mouse monoclonal anti-sarcomeric α-actinin primary antibody (isotype: IgM; Cat. No.: ab49672) and Alexa Fluor 488 polyclonal goat anti-mouse IgM secondary antibody (Cat. No.: ab150121) were bought from Abcam. N-(β-maleimidopropyloxy) succinimide ester (BMPS, Cat. No.: F01022) was ordered from Highfine Biotech (Suzhou, China). The rest chemicals were acquired from Sigma-Aldrich unless otherwise stated.

Modification of BSA: BSA (1.33 g, 0.02 mmol) was dissolved in Na$_2$HPO$_4$ solution (50 mL, 100×10^{-3} M) under agitation. Subsequently, BMPS (532.4, 425.9, 319.5, 213.0, or 106.5 mg; 2, 1.6, 1.2, 0.8, or 0.4 mmol) was added and the reaction was carried out at ambient temperature in the dark for 6 h. After that, the mixture was transferred to a dialysis bag (12–14 kD MWCO tubing, Spectra/Por 4, Spectrum Laboratories Inc.) and dialyzed against ultrapure water (NANOpure Water Purification System, Thermo Scientific Barnstead, 2 L × 10) for 3 d. The newly purified protein solution was concentrated by centrifugal

filtration using two types of centrifugal filters (preliminary enrichment: Cat. No.: 4304, Centriprep, 10 kD MWCO, Millipore; advanced enrichment: Cat. No.: UFC500396, Amicon Ultra, 3 kD MWCO, Millipore) in succession to a final concentration of larger than 120 mg mL^{-1}. Subsequently, the protein solution was flash frozen in liquid nitrogen and immediately stored in a −80 °C freezer (MDF-U76VC, SANYO) for later use. The mass concentration was determined by weighing the solid in a protein solution (500 μL) in a 1.5 mL glass vial (GL Sciences) after lyophilization. As a control, BSA without modification but dialyzed and concentrated under the same condition was prepared.

Proton Nuclear Magnetic Resonance (^{1}H-NMR) Spectroscopy: The ultrapure water in the protein solutions was replaced by D$_2$O in centrifugal filters after repeated concentration and replenishment with D$_2$O. Afterwards, the protein solutions were further diluted in D$_2$O to a final concentration of around 10 mg mL^{-1}. The ^{1}H-NMR spectra of the freshly prepared specimens were immediately determined on a 400 MHz NMR spectrometer (Avance II, Bruker) with scan times of at least 64 in order to obtain high signal-to-noise (SNR) ratios. The spectra were calibrated by setting the chemical shift (δ) of HOD to be 4.8 ppm.

Dynamic Light Scattering (DLS): Protein solutions were diluted in phosphate buffered saline (PBS) (137×10^{-3} M NaCl, 2.7×10^{-3} M KCl, 10×10^{-3} M Na$_2$HPO$_4$, 1.8×10^{-3} M KH$_2$PO$_4$, pH = 7.4) to 1 mg mL^{-1}, which were passed through 0.22 μm syringe filters (Cat No.: SLGP033RS, Millex, Millipore). The hydrodynamic size of protein was measured on a DLS analyzer (ZetaPALS, Brookhaven Instruments).

Sodium Dodecyl Sulfate Polyacrylamide Gel Electrophoresis (SDS-PAGE): Protein solutions were diluted in ultrapure water to 1 mg mL^{-1} and mixed (1:1) with SDS loading buffer (2×, pH ≈ 6.8) containing tris(hydroxymethyl)aminomethane hydrochloride (Tris-HCl) (100×10^{-3} M), SDS (4 w/v%), bromophenol blue (0.2 w/v%), glycerol (20 v/v%) and β-mercaptoethanol (200×10^{-3} M). The samples were loaded on a separating gel (12 w/v%) and a prestained protein marker (Cat No.: 26616, PageRuler, Thermo Scientific Pierce) was applied as the standard for molecular weight. The electrophoresis (power supply: EPS 3501 XL, GE Healthcare Life Sciences) was performed at 250 V and 35 mA for 70 min using Tris-Glycine running buffer (25×10^{-3} M Tris, 192×10^{-3} M glycine, 0.1 w/v% SDS). Afterwards, the samples were stained with brilliant blue (0.5 w/v%) in a mixed solution of ethanol (50 v/v%), H$_2$O (40 v/v%), and acetic acid (10 v/v%) for 2 h and washed (75 v/v% H$_2$O, 15 v/v% ethanol, and 10 v/v% acetic acid) for 1 h. The separating gel was then photographed on an imaging system (SmartView Pro 1100 Imager System, Major Science).

Circular Dichroism (CD) Spectroscopy: Protein solutions were diluted in PBS to 0.2 mg mL^{-1} and their equilibrium CD spectra were measured at room temperature using a spectropolarimeter (J-810, JASCO) with a quartz cuvette. All the spectra were averaged over three scans from 200 to 320 nm at an interval of 1 nm. Scanning mode was continuous and the speed was 20 nm min^{-1}. The mean residue ellipticity (θ_{MRE}) was computed using the equation (Equation (1))

$$\theta_{MRE} = \frac{\theta \cdot M}{c \cdot l \cdot N} \tag{1}$$

where θ is the measured ellipticity, M is the protein molecular weight, c is the protein concentration (0.2 mg mL^{-1}), l is the path length (0.1 cm), and N is the number of amino acid residues in a protein. The contents of α-helix and β-sheet in BSA were estimated based on the CD spectral data using CDPro software package.

Study on Gelation Formulations: Pristine, dialyzed or modified BSA solution (100 mg mL^{-1} in 100×10^{-3} M Na$_2$HPO$_4$, pH ≈ 7.5) was fully mixed with RRP solution (100 mg mL^{-1} in 140×10^{-3} M NaOH solution, pH ≈ 7.5) at varying ratios in a 1.5 mL glass vial at ambient temperature and then kept still in dark. At preseted time points (1 and 12 h), the vial was inverted and the physical state of hydrogel was recorded.

Scanning Electron Microscopy (SEM): Hydrogel precursor solution (50 μL) was casted in a well (8 mm in diameter and 1 mm in depth) formed from a perforated plastic plate laid on a polydimethylsiloxane (PDMS) membrane and incubated in a humidified metal box for 24 h

www.MaterialsViews.com

ADVANCED
FUNCTIONAL
MATERIALS
www.afm-journal.de

FULL PAPER

at ambient temperature. The as-prepared hydrogel disks were flash frozen in liquid nitrogen and immediately freeze-dried, which shrank and cracked automatically after lyophilization. The desiccated hydrogel pieces were then mounted on the inclined plane of an angled (60°) metal stub with the inner cross-sections at cracks upward. Afterwards, the specimens were deposited with a 15 nm gold layer in a gold sputter coater (S150B, Edwards) and observed under a scanning electron microscope (SEM, JSM 6490, JEOL). Images were taken at 10 kV accelerating voltage and 500× or 2000× magnification.

Dynamic Mechanical Analysis (DMA): Hydrogel was prepared as before and transferred to a parallel plate fixture (8 mm in diameter) mounted on a rheometer (ARES, TA Instruments). The upper plate was slowly moved down against the hydrogel until an axial force of around 15 g was applied. The shear test (time scan mode) for hydrogel stiffness was performed at 5% strain and 10 rad s^{-1} frequency. The dynamic mechanical tests for the three representative hydrogels and those crosslinked using dithiothreitol (DTT) were carried out at strain sweep mode (1% to 100% strain at 10 rad s^{-1} frequency) and frequency sweep mode (1 to 100 rad s^{-1} frequency at 5% strain).

Swelling Behavior of Hydrogel: Hydrogel precursor solution (50 µL) was placed in a closed 1.5 mL plastic tube (Cat. No.: MCT-150-C, Axygen, Corning Life Sciences) and the mass of it was obtained by subtracting the mass of empty tube from that of loaded one. After gelation for 24 h, 1 mL PBS solution was added and the hydrogel was immersed in it for 24 h, during which the PBS solution was renewed once after 12 h. Subsequently, PBS solution was carefully removed and the mass of hydrogel after swelling was determined. The water uptake capability (C) of hydrogel is defined as (Equation (2))

$$C = \frac{m_t - m_0}{m_0} \times 100\% \qquad (2)$$

where m_t and m_0 are the masses of hydrogel after and before swelling, respectively.

Tensile Test: Hydrogel precursor solution (130 µL) was casted in a dumbbell-shape mold (dimension for the middle part: 10 × 4 mm; dimension for both ends: 5 × 6 mm; depth: 1.25 mm) formed from a custom-made perforated plastic plate laid on a PDMS membrane and incubated in a humidified metal box for 24 h at ambient temperature as before. The as-prepared hydrogel was transferred onto a thin film fixture mounted on the rheometer. Two self-made PDMS spacer pieces with complementary shape to the ends of hydrogel were used as clamps, which were fixed on the fixture with sticky tape so that the axial force would be loaded onto the middle part of hydrogel. Tensile test was performed by stretching the hydrogel at a rate of 0.05 mm s^{-1} to a preset strain of 100%.

Cell Culturing and Harvesting: C2C12 (Mouse myoblast cell line, CRL-1772, ATCC) cells were raised on a culture dish in DMEM (10 mL) supplemented with NaHCO$_3$ (3.7 g L^{-1}), FBS (20 v/v%) and P/S (1 v/v%). The Cells were incubated at 37 °C with 5% CO$_2$ and the culture medium was renewed every day until the confluence of them reached to around 80%. Subsequently, the medium was replaced by PBS (5 mL). After 5 min incubation, PBS was removed and trypsin (0.05 w/v%)/EDTA (0.53 × 10^{-3} M) solution (1 mL) was added. The cells were placed back in the incubator again until thoroughly detached with gentle shake. Following that, culture medium (9 mL) was replenished and the cells were either used for passage or for 3D encapsulation in the hydrogel.

3D Cell Encapsulation: RRP and RGDC peptide (100 mg for each) were weighted in a 1.5 mL plastic tube individually and then suspended in diethyl ether and deposited by centrifugation. Then the supernatant solution was carefully removed so as to avoid the loss of solid. The purification procedure was repeated for several times, after which the remaining organic solvent was eliminated by freeze-drying. Subsequently, both peptides were dissolved in water (860 µL for RRP and 680 µL for RGDC) with pH adjusted to ≈7.5 using NaOH (1 M) solution (140 µL for RRP and 320 µL for RGDC). The harvested cells were deposited by centrifugation and resuspended in BSA-BMPS(12.0) solution to a density of about 10^6 cells mL^{-1}. To form 3D cell-encapsulated hydrogel,

the cell suspension (48 µL) was well blended with RRP or RRP/RGDC (98 wt%/2 wt%) solution (12 µL) at a volume ratio of 8:2 in a 1.5 mL plastic tube and then quickly transferred into a 96-well plate (TPP). Following the formation of hydrogel, cell culture medium (DMEM with 2 v/v% HS instead of 20 v/v% FBS, 150 µL) was added. The medium was renewed every 12 h in the first two days and then once every day until used.

Viability Test of Cells: At day 7, cells encapsulated in the protein hydrogel matrix were stained with FDA/PI solution (10 µg mL^{-1} in cell culture medium for both, 150 µL) for 30 min. After washing with PBS for three times, the samples were carefully fetched out with a small stainless scoop and placed onto a glass coverslip with the upside down. Fluorescence images were immediately taken using a confocal laser scanning microscope (CLSM, TCS SP5 II, Leica). Images were processed with Imaris (Bitplane, Northern Ireland) and the viability of cells was calculated by comparing the relative volume of live cells (green ones) to the total volume of cells (green and red ones).

Immunostaining of Cells: Also at day 7, other specimens were fixed with paraformaldehyde (4% in PBS, 150 µL) for 2 h, permeabilized with Triton X-100 (0.2% in PBS, 150 µL) for 2h and then blocked with BSA (5% in PBS, 150 µL) for overnight. Subsequently, they were washed with PBS for one time before incubation with mouse monoclonal anti-sarcomeric α-actinin primary antibody (100× dilution in PBS, 150 µL) for 12 h. After that, they were rinsed with PBS again and then stained with Alexa Fluor 488 polyclonal goat anti-mouse IgM secondary antibody (100× dilution in PBS, 150 µL) for another 12 h. The filamentous actin (F-actin) and nuclei of cells were simultaneously stained with rhodamine-labeled phalloidin (100× dilution in PBS) and DAPI (10 µg mL^{-1} in PBS) for 12 h again. The samples were extensively rinsed and immersed in PBS for a whole day prior to being placed onto a coverslip as before. Fluorescence images for immunostaining were taken using a CLSM (LSM 710, Zeiss) and processed with Imaris as well.

Statistical Analysis: Experimental data were presented as mean ± std or mean ± sem. Statistical significance was calculated by Welch's t-test with a homemade program in Matlab R2013b (The MathWorks).

Supporting Information

Supporting Information is available from the Wiley Online Library or from the author.

Acknowledgements

[1] a) E. S. Place, N. D. Evans, M. M. Stevens, *Nat. Mater.* **2009**, *8*, 457; b) F. J. O'Brien, *Mater. Today* **2011**, *14*, 88; c) V. Mironov, R. P. Visconti, V. Kasyanov, G. Forgacs, C. J. Drake, R. R. Markwald, *Biomaterials* **2009**, *30*, 2164; d) V. Mironov, V. Kasyanov, C. Drake, R. R. Markwald, *Regener. Med.* **2008**, *3*, 93; e) S. V. Murphy, A. Atala, *Nat. Biotechnol.* **2014**, *32*, 773.

[2] R. Lanza, R. Langer, J. Vacanti, *Principles of Tissue Engineering*, Academic Press, Boston, MA **2007**.

[3] T. G. Kim, H. Shin, D. W. Lim, *Adv. Funct. Mater.* **2012**, *22*, 2446.

[4] C. E. Murry, G. Keller, *Cell* **2008**, *132*, 661.

[5] A. Atala, F. K. Kasper, A. G. Mikos, *Sci. Transl. Med.* **2012**, *4*, 160rv12.

[6] D. T. Butcher, T. Alliston, V. M. Weaver, *Nat. Rev. Cancer* **2009**, *9*, 108.

[7] a) D. E. Discher, P. Janmey, Y.-L. Wang, *Science* **2005**, *310*, 1139; b) M. P. Lutolf, P. M. Gilbert, H. M. Blau, *Nature* **2009**, *462*, 433; c) Y. Chen, J. Wang, B. Shen, C. W. Y. Chan, C. Wang, Y. Zhao, H. N. Chan, Q. Tian, Y. Chen, C. Yao, I.-M. Hsing, R. A. Li, H. Wu, *Macromol. Biosci.* **2015**, *15*, 426.

[8] a) M. W. Tibbitt, K. S. Anseth, *Biotechnol. Bioeng.* **2009**, *103*, 655; b) S. Van Vlierberghe, P. Dubruel, E. Schacht, *Biomacromolecules* **2011**, *12*, 1387; c) N. Annabi, A. Tamayol, J. A. Uquillas, M. Akbari, L. E. Bertassoni, C. Cha, G. Camci-Unal, M. R. Dokmeci, N. A. Peppas, A. Khademhosseini, *Adv. Mater.* **2014**, *26*, 854; d) S. W. Liao, T.-B. Yu, Z. Guan, *J. Am. Chem. Soc.* **2009**, *131*, 17638; e) S. W. Liao, J. Rawson, K. Omori, K. Ishiyama, D. Mozhdehi, A. R. Oancea, T. Ito, Z. Guan, Y. Mullen, *Biomaterials* **2013**, *34*, 3984.

[9] a) J. Kopeček, J. Yang, *Angew. Chem. Int. Ed.* **2012**, *51*, 7396; b) R. L. DiMarco, S. C. Heilshorn, *Adv. Mater.* **2012**, *24*, 3923.

[10] a) A. I. Van Den Bulcke, B. Bogdanov, N. De Rooze, E. H. Schacht, M. Cornelissen, H. Berghmans, *Biomacromolecules* **2000**, *1*, 31; b) C. T. S. Wong Po Foo, J. S. Lee, W. Mulyasasmita, A. Parisi-Amon, S. C. Heilshorn, *Proc. Natl. Acad. Sci. USA* **2009**, *106*, 22067; c) J. W. Nichol, S. T. Koshy, H. Bae, C. M. Hwang, S. Yamanlar, A. Khademhosseini, *Biomaterials* **2010**, *31*, 5536;

d) N. Annabi, K. Tsang, S. M. Mithieux, M. Nikkhah, A. Ameri, A. Khademhosseini, A. S. Weiss, *Adv. Funct. Mater.* **2013**, *23*, 4950; e) Y. Gao, Q. Luo, S. Qiao, L. Wang, Z. Dong, J. Xu, J. Liu, *Angew. Chem. Int. Ed.* **2014**, *53*, 9343; f) D. Yuan, X. Du, J. Shi, N. Zhou, J. Zhou, B. Xu, *Angew. Chem. Int. Ed.* **2015**, *54*, 5705; g) F. Sun, W.-B. Zhang, A. Mahdavi, F. H. Arnold, D. A. Tirrell, *Proc. Natl. Acad. Sci. USA* **2014**, *111*, 11269; h) X. Shi, S. Ostrovidov, Y. Zhao, X. Liang, M. Kasuya, K. Kurihara, K. Nakajima, H. Bae, H. Wu, A. Khademhosseini, *Adv. Funct. Mater.* **2015**, *25*, 2250.

[11] a) B. H. Northrop, R. N. Coffey, *J. Am. Chem. Soc.* **2012**, *134*, 13804; b) Z. Liu, C. Dong, X. Wang, H. Wang, W. Li, J. Tan, J. Chang, *ACS Appl. Mater. Interfaces* **2014**, *6*, 2393; c) R. Qiao, C. Liu, M. Liu, H. Hu, C. Liu, Y. Hou, K. Wu, Y. Lin, J. Liang, M. Gao, *ACS Nano* **2015**, *9*, 2120.

[12] a) C. M. Elvin, A. G. Carr, M. G. Huson, J. M. Maxwell, R. D. Pearson, T. Vuocolo, N. E. Liyou, D. C. C. Wong, D. J. Merritt, N. E. Dixon, *Nature* **2005**, *437*, 999; b) S. Lv, D. M. Dudek, Y. Cao, M. M. Balamurali, J. Gosline, H. B. Li, *Nature* **2010**, *465*, 69.

[13] G. Qin, X. Hu, P. Cebe, D. L. Kaplan, *Nat. Commun.* **2012**, *3*, 1003.

[14] a) E. Ruoslahti, M. D. Pierschbacher, *Science* **1987**, *238*, 491; b) U. Hersel, C. Dahmen, H. Kessler, *Biomaterials* **2003**, *24*, 4385.

[15] a) B. Trappmann, J. E. Gautrot, J. T. Connelly, D. G. T. Strange, Y. Li, M. L. Oyen, M. A. C. Stuart, H. Boehm, B. J. Li, V. Vogel, J. P. Spatz, F. M. Watt, W. T. S. Huck, *Nat. Mater.* **2012**, *11*, 642; b) J. H. Wen, L. G. Vincent, A. Fuhrmann, Y. S. Choi, K. C. Hribar, H. Taylor-Weiner, S. Chen, A. J. Engler, *Nat. Mater.* **2014**, *13*, 979.

[16] U. Kragh-Hansen, *Pharmacol. Rev.* **1981**, *33*, 17.